Mn-doped Fe_2O_3-$ZnFe_2O_4$ Composites for High Performance Lithium Ion Battery Anodes

Lixia Liao[*]*, Tao Fang, Shuai Zhan, Dehui Weng*

Department of Chemistry, College of Science, Northeast Forestry University, Harbin 150040, China
[*]E-mail: lxliao1024@126.com

Mn-doped nanocrystallines $ZnFe_2O_4$ in various proportions have been successfully carried out by self-propagating combustion method. The morphologies and electrochemical performance of the samples obtained were analyzed by X-ray diffraction (XRD), scanning electron microscopy (SEM), constant-current charge-discharge, cyclic voltammetry (CV) and electrochemical impedance spectroscopy (EIS). The results show that the electrode that the proportion of Mn to Zn is 7:3 in the as-synthesized sample exhibits the highest initial discharge specific capacity of 1692.0 mAh g^{-1} and charge capacity of 1059.4 mAh g^{-1}. Moreover, the outstanding cycling stability is obtained with a 774.1 mAh g^{-1} capacity retention at a current density of 60 mA g^{-1} after 20 cycles, which is obviously higher than that of electrode without Mn-doping of 468.2 mAh g^{-1}. The excellent electrochemical properties are ascribed to a faster lithium intercalation kinetic process.

1. INTRODUCTION

Lithium ion battery has been widely used in various portable electronic devices such as mobile phones, digital cameras and notebook computers because it possesses characteristics of light weights, stable output voltage and environmental friendliness etc. Nowadays, it has shown broad prospect of application in high-power fields such as hybrid electric vehicles and plug-in electric vehicles. Graphite is one of commercial anode materials for lithium ion battery owing to its abundance, low cost, longer cycle life and environmental friendliness. However, the theory capacity is only 372 mAh g^{-1}, and it also poses safety problems that Li metal can deposit on the graphite anode when the battery was charged at high current density[1,2]. All of these problems stimulate researchers to look for novel anode materials with high energy density, low cost and longevity.

Transitional metal oxides have been studied as lithium ion battery anode in the past decade because it has a series of virtues such as high volumetric energy density, easy availability and environmental benignity [2-6]. Moreover, $ZnFe_2O_4$ can storage 8-10 units lithium ion per elementary unit due to coexistence reaction mechanism with alloying-dealloying reaction and oxidation-reduction reaction mechanism, and the theoretical capacity can reach to 1072 mAh g^{-1} [7]. α-Fe_2O_3 has high oxide state, and the theory capacity can reach to 1005 mAh g^{-1} based on oxidation-reduction storage lithium mechanism [8]. However, the conductivity of the materials is lower and their working voltage is higher, doping modification is one of effective ways to ameliorate the problem. Mn_3O_4 has a discharge voltage plateau of 0.5 V (*vs*. Li/Li$^+$) and a charge voltage plateau of 1.25 V (*vs*. Li/Li$^+$) [9], which are lower than that of $ZnFe_2O_4$ (discharge:0.8 V *vs*. Li/Li$^+$, charge:1.5 V *vs*. Li/Li$^+$). Mn_3O_4 nanosheets exhibit a lower discharge voltage of 0.25 V than $ZnFe_2O_4$, and show a higher reversible capacity of 520 mAh g^{-1} [10] to compensate the low capacity of ZnO (400 mAh g^{-1}), which is ascribed to low electronic conductivity of ZnO particles and the large volume change in chare/discharge process [11]. Mn doping nanomaterials prepared by electrospun method can improve the reversible capacity and lower the working voltage to some extent [12].

Herein, we report a facile self-propagating combustion method to synthesize Mn-doped Fe_2O_3-$ZnFe_2O_4$ composites. The electrochemical tests showed that the Mn-doped Fe_2O_3-$ZnFe_2O_4$ nano material is predicted to possess the higher reversible capacity and the lower working voltage.

2. EXPERIMENTAL

2.1. Synthesis

All of the reagents are of analytical purity and used without further purification. $ZnFe_2O_4$ nanomaterials based on sol-gel self-propagating combustion were prepared as follows: 25 mmol of $Zn(NO_3)_2 \cdot 6H_2O$ and 50 mmol of $Fe(NO_3)_3 \cdot 9H_2O$ were solved in distilled water to prepare a precursor solution, and citric acid was slowly added into the above solution followed by magnetic stirring. After the homogeneous solution was obtained, the pH value of mixture was controlled at 7.0 by ammonia solution, and then the solution was concentrated in a beaker under thermostats magnetic stirring at about 60 °C. The solution was gradually contrated, and then a brown wet gel was slowly formed. The gel concentrated in a crucible was dried in 120 °C oven, and a brown honeycomb gel was formed. Finally the drying gel was heated on the electric fire, when gel temperature was reached to critical temperature, a great deal of foams and a spark appeared at one corner, and then spread throughout the mass, yielding a brown voluminous and fluffy product in the container. And finally annealed at 700 °C for 2 h, the product was marked as ZF.

Mn-doped Fe_2O_3-$ZnFe_2O_4$ composites were prepared according to the above methods, 7.5, 12.5 and 17.5 mmol $Mn(NO_3)_2$ was used to substitute part of $Zn(NO_3)_2 \cdot 6H_2O$, and the corresponding products were labeled as ZMF1, ZMF2 and ZMF3, respectively.

2.2. Characterization

The crystal structure of the materials was characterized by X-ray diffraction (XRD, PANalytical X'Pert PRO) with nickel-filtered Cu Kα radiation. The morphology was determined by the scanning electron microscopy (SEM, Hitachi S4700).

2.3. Electrochemical performance

The composite electrodes were fabricated on a mass ration of 60% Mn-doped (without Mn-doped) Fe_2O_3-$ZnFe_2O_4$ composites, 25% acetylene black and 15% polyvinylidene difluoride (PVDF), moderate amount of N-methyl-2-pyrrolidone (NMP) was added to the above the mixture to adjust the viscosity of slurry, and then the slurry was coated on copper foil. After the electrode was dried at 120 °C for 12 h, and then punched into circular discs. Finally, the composite electrodes were dried under vacuum at 80 °C for 10 h. The 2025 coin-type cells were assembled with the composite electrode as work electrode, and lithium plate as counter electrode, and the mixture solution of 1 M $LiPF_6$ in ethylene carbonate/diethyl carbonate (1:1 v/v)/ solution as electrolyte. The whole assemble process was carried out in an argon-filled glove box. The electrochemical measurements were evaluated by battery test system (Neware BTS-610) at a current density of 60 mA g^{-1} in the voltage range of 0.01-3.0 V (vs. Li/Li$^+$). In this report, the lithiation was expressed as discharging, whereas the de-lithiation as charging. Cyclic voltammetry (CV) and electrochemical impedance spectroscopy (EIS) measurements were performed by a three-electrode electrochemical cell, and lithium metal foil and wire were used as reference and counter electrodes using electrochemical workstation (Shanghai Chenhua Instrument Co.). CV measurements were recorded at a scan rate of 0.1 mV/s within a voltage window of 0.01-3.0 V, and EIS tests were determined over a frequency range of 10^{-2}-10^5 Hz with an ac voltage signal of ±5 mV. The obtained impedance spectras were fitted by the ZsimpWin300 Program.

3. RESULTS AND DISCUSSION

3.1. XRD analysis
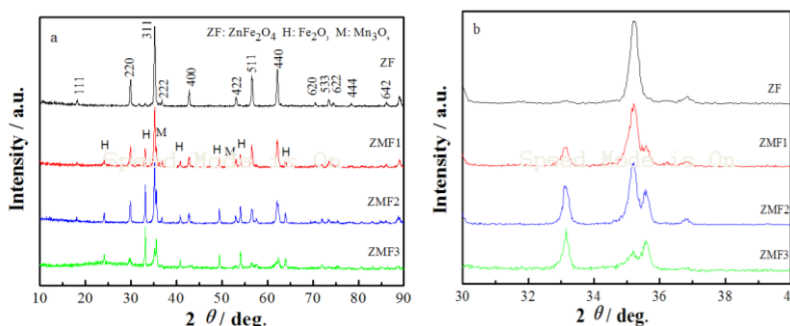
Figure 1. X-ray diffraction patterns (a) and magnified (311) peaks of Zn ferrites powers with different Mn contents (b).

Fig. 1 showed the XRD patterns of ZF, ZMF1, ZMF2, and ZMF3 nanomaterials obtained after sintering process. As shown in Fig. 1(a), characteristic peaks of $ZnFe_2O_4$ (JCPDS 22-1012) were identified in the pattern of ZF material, and extra diffraction peaks of hematite (α-Fe_2O_3, JCPDS 79-1741) were identified in the patterns of ZMF1, ZMF2 and ZMF3 nanomaterials. The intensity ration of the peak (2θ=35.3°) of $ZnFe_2O_4$ to that (2θ=33.2°) of α-Fe_2O_3 was decreased drastically with increasement of Mn, disclosing that Mn doping could significantly weaken the formation of $ZnFe_2O_4$ and enhance the formation of α-Fe_2O_3. It is worthy mentioning that a slightly peak splitting phenomenon was observed in Fig. 1(b), indicating that another new phase may be formed. The splitting phenomenon was more obvious with increasement of Mn doping. Therefore, it was concluded that Mn doping could significantly affect the phase composition of the mixed oxides.

3.2. SEM analysis
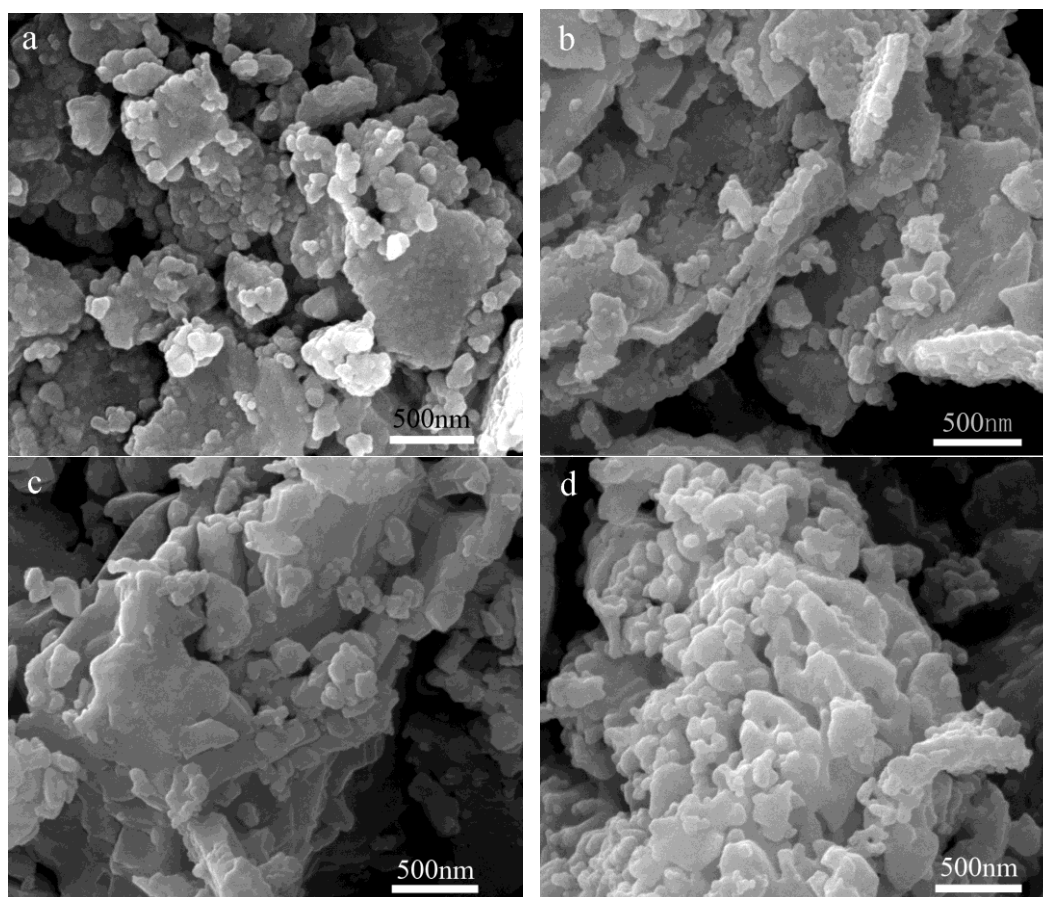
Figure 2. SEM of ZF(a), ZMF1(b), ZMF2(c) and ZMF3 (d) nanomaterials.

The morphologies of all samples for different Mn content are shown in SEM micrographs of Fig. 2. Fig. 2(a-d) represents the as-prepared samples of ZF, ZMF1, ZMF2, and ZMF3 nanomaterials, respectively. Almost all the samples display the hetergeneous surface morphology, and the particle sizes were distributed in the range of 30 nm to 80 nm. However, when $Mn(NO_3)_2$ was doped, the particle size distribution and particles agglomeration have changed, indicating that the Mn doping can

influence particles morphology, and finally can greatly influence the electrochemical performance of the materials. It is worth mentioning that the morphology of ZMF3 nanomaterial is relatively uniform and almost no obvious agglomerates can be observed.

3.3. Electrochemical performance

The electrochemical properties of ZF, ZMF1, ZMF2 and ZMF3 nanoparticles were evaluated by galvanostatic discharge/charge cycling within the voltage range of 0.01-3.0 V at the current density of 60 mA g^{-1}. The first discharge/charge curves of the samples were shown in Fig.3. The discharge capacities of ZF, ZMF1, ZMF2 and ZMF3 were 874.6, 1396.6, 1512.4 and 1692.0 mAh g^{-1}, respectively. It can be seen that the Mn doping could obviously enhance first discharge capacity, and ZMF3 demonstrates the highest discharge and charge capacity of 1692.0 and 1059.4 mAh g^{-1}, respectively. The high specific capacity of ZMF3 nanoparticles may be due to homogeneous surface morphology. Secondly, the nanoparticles with Mn doping can transform into another new phase, which can decrease the interface resistance. Moreover, the proper exaggerated lattice parameters may play an important part in delaying the capacity loss [13]. Similar phenomena of new phase formation have been observed for NiFe$_2$O$_4$ and CuFe$_2$O$_4$ transition metal oxides [14,15]. The higher initial reversible capacities loss of all samples was mainly attributed to the incomplete electrochemical reaction.

The cycling performance of the electrodes was illustrated in Fig. 3(b) at a current density of 60 mA g^{-1} for 20 cycles. It is obvious that the ZMF3 electrode exhibits much higher reversible capacity and better cycling stability. After 20 cycles, the ZMF3 electrode shows the highest reversible capacity of 774.1 mAh g^{-1}. In contrast, the reversible capacities of ZF, ZMF1 and ZMF2 electrodes are 468.2, 660.0 and 605.6 mAh g^{-1}.
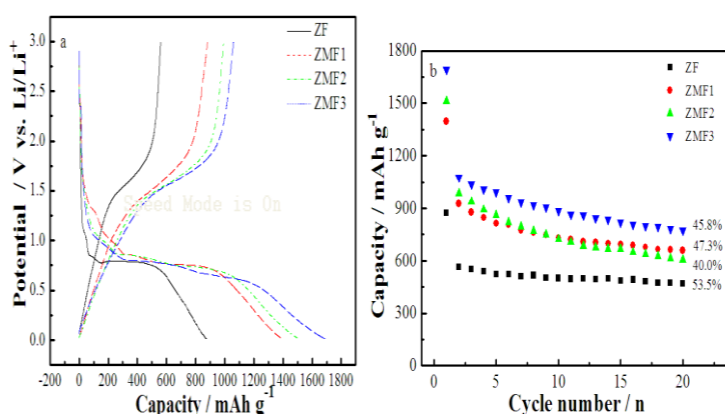
Figure 3. Charge/discharge curve(a) and cycling performance(b) of ZF, ZMF1, ZMF2 and ZMF3 electrodes.

To further investigate the electrochemical performance, the cyclic voltammetry (CV) profiles of the electrodes were presented in Fig.4. There is a substantial difference between the first and the

subsequent cycles. In the first negative sweep, two small peaks at 1.1 V and 0.8 V were observed, which is ascribed to the Li-intercalation process involved the reduction of Fe(III) in $ZnFe_2O_4$ to form the intercalation phase $Li_xZnFe_2O_4$ [2], the cathodic peak at around 0.55 V in the first cycle can be assigned to the reduction reaction of $ZnFe_2O_4$ with Li into Zn and Fe, and the further lithiation of Zn to give a Li-Zn alloy [16]. It is worthy mentioning that for the material without Mn doping, the symmetry of the peak located at 0.55 V is better. However, the peaks of the nanoparticles with Mn doping appeared the slight splitting phenomenon, and the splitting phenomenon became more and more seriously. When the amount of Mn doping increased to 17.5 mmol, the peak around 0.5 V thoroughly split into two peaks. These indicate that Mn doping affects the mechanism of intercalation/deintercalation mechanism to some extent. The reaction mechanism needs to further investigate. An anodic peak located at around 1.6 V in the first cycle might be attributed to the oxidation of Zn^0 and Fe^0 [17] and Mn^0. During the subsequent cycles, the cathodic peak shifts to 0.85-0.90 V, which is indicative of reduction of metal oxide. In the third cycle, cathodic peak potential of Mn-doping sample is around 0.82 V, that of ZF nanomaterial without Mn-doping is about 0.90 V, indicating that Mn doping can successfully bring down the working voltage. This is analogue to the report by Zu et al. [12].

Electrochemical impedance spectroscopy has been performed to get insight about the difference in electrochemical performance for ZF, ZMF1, ZMF2 and ZMF3 materials. The measurements were carried out after 50 cycles. The equivalent circuit was demonstrated in the inset of Fig. 5.
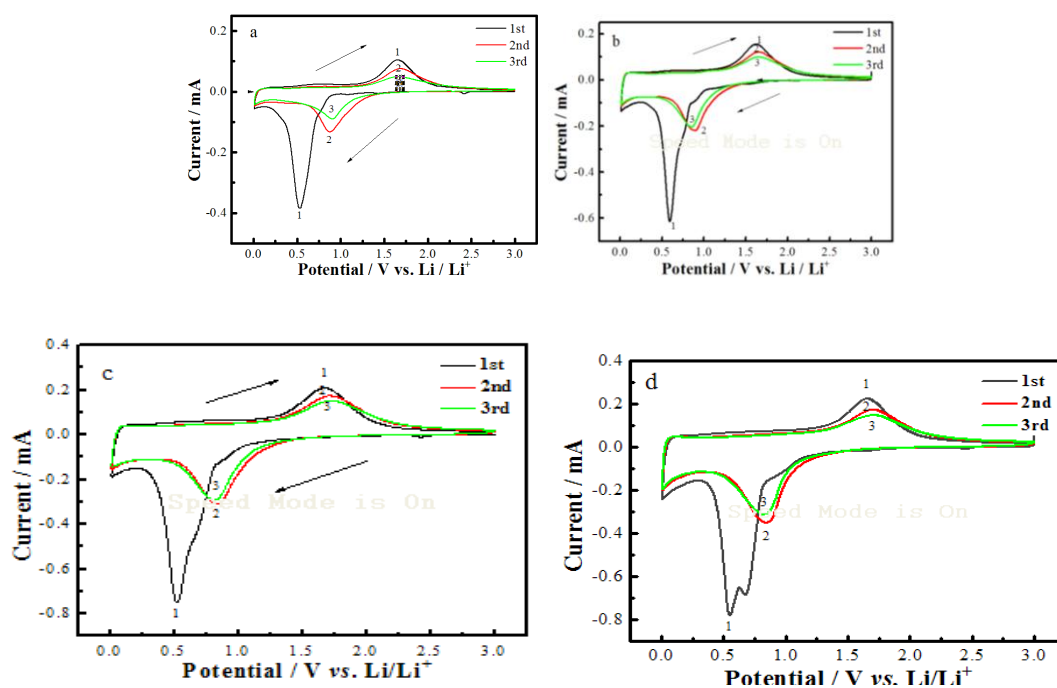
Figure 4. Cyclic voltammetry profiles of ZF(a), ZMF1(b), ZMF2(c) and ZMF3(d) electrodes.

As it was described in the related research work [18,19], R is the ohmic resistance, corresponding to the intercept at the real (Z') axis in high frequency. CPE and R_{ct} are the constant phase element and charge transfer resistance at the electrode/electrolyte interface, corresponding to the semicircle in the middle frequency range. W is the Warburg impedance related to the diffusion of ions in the bulk electrode, indicated by a straight sloping line at the low frequency region of the Nyquist plots. The fitted impedances using the proposed equivalent circuit are shown by the solid lines in Fig. 5. The charge transfer resistance values of ZF, ZMF1, ZMF2 and ZMF3 were 70.81, 46.02, 41.1 and 36.91 Ω, respectively, indicating that a fast lithium intercalation kinetic process is occurred at the surface of ZMF3 electrode, which is ascribed to the material with the higher reactivity activity.
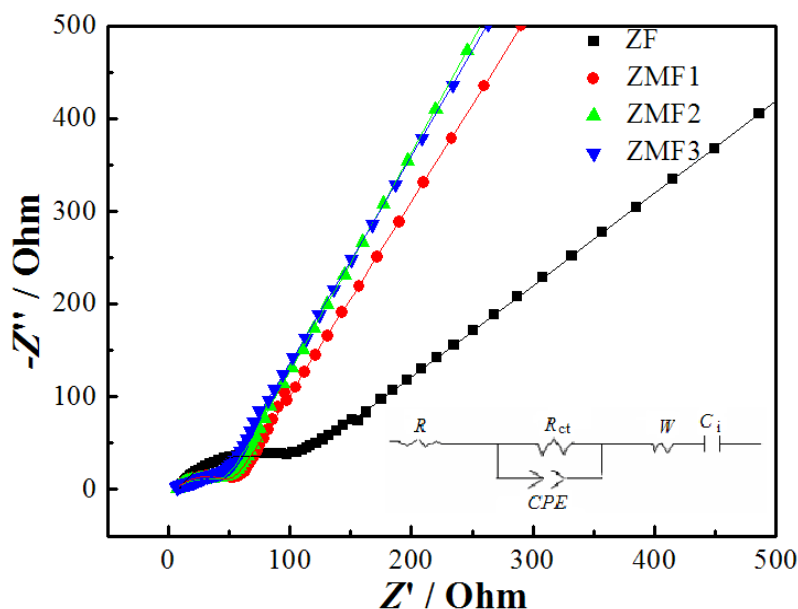
Figure 5. Electrochemical impedance spectroscopys of the ZF, ZMF1, ZMF2 and ZMF3 electrodes.

4. CONCLUSION

Mn-doped nanocrystallines $ZnFe_2O_4$ in various proportions were efficiently synthesized by self-propagating combustion method, and the effect of Mn doping on composition and electrochemical performance of zinc ferrites were demonstrated. Mn-dopped zinc ferrites can bring down the working voltage and improve the reversible capacity, which is ascribed to the formation of α-Fe_2O_3-$ZnFe_2O_4$ composites, and it can decrease the charge transfer resistance, accelerate the electrochemical reaction rate. As the ratio of manganese nitrate to zinc nitrate is 7:3, the electrode can demonstrate the reversible capacity of 774.1 mAh g^{-1} after 20 cycles.

References

1. C. Uhlmann, J. Illiga, M. Endera, R. Schuster and E. Ivers-Tiffée, *J. Power Sources*, 279 (2015) 428.
2. A. S. Hameed, H. Bahiraei, M.V. Reddy, M.Z. Shoushtari, J.J. Vittal, C.K. Ong and B.V.R. Chowdari, *ACS Appl. Mater. Interfaces*, 6 (2014) 10744.
3. L. M. Yao, X. H. Hou, S. J. Hu, Q. Ru, X. Q. Tang, L. Z. Zhao and D. W. Sun, *J. Solid State Electrochem.*, 17 (2013) 2055.
4. Z. Xing, Z. C. Ju, J. Yang, H. Y. Xu and Y. T. Qian, *Electrochim. Acta*, 102 (2013) 51.
5. Z. L. Zhang, Y. H. Wang, Q. Q. Tan, Z. Y. Zhong and F .B. Su, *J. Colloid Interf. Sci.*, 398 (2013) 185.
6. Z. C. Bai Y. W. Zhang, Y. H. Zhang, C. L. Guo and B. Tang, *Electrochim. Acta*, 159 (2015) 29.
7. L. Lin and Q. M. Pan, *J. Mater. Chem. A*, 3 (2015) 1724.
8. Y.X. Chen, L. Zhang, L.H. He, Y.D. He, P.J. Shang, Z.Q. Liu and H.B. Liu, *Mater. Lett.*, 75 (2012) 2   3   .
9. M.H. Alfaruqi, J. Gim, S. Kim, J.J. Song, P.T. Duong , J. Jo, J.P. Baboo, Z.L. Xiu, V. Mathew and J. Kim, *Chem. Eur. J.*, 22 (2016) 2039.
10. M.M. Zhen, Z. Zhang, Q.T. Ren and L. Liu, *Mater. Lett.*, 177 (2016) 21.
11. H. Wang, Q. Pan, Y. Cheng, J. Zhao and G. Yin, *Electrochim. Acta*, 54 (2009) 2851.
12. C.X. Zu and H. Li, *Energy Environ. Sci.*, 4 (2011) 2614.
13. X.Q. Tang, X.H. Hou, L.M. Yao, S.J. Hu, X. Liu and L.Z. Xiang. *Mater. Res. Bull.*, 57 (2014) 127.
14. S. Balaji, R. Vasuki and D. Mutharasu, *J. Alloys Compd.*, 554 (2013) 5.
15. Y.S. Fu, Q. Chen, M.Y. He, Y.H. Wan, X.Q. Sun, H. Xia and X. Wang, *Ind. Eng. Chem. Res.*, 51 (2012) 11700.
16. Z. Xing, Z.C. Ju, J. Yang, H.Y. Xu and Y.T. Qian, *Nano Res.*, 5 (2012) 477.
17. F. Zou, X.L. Hu, Z. Li, L. Qie, C.C. Hu, R. Zeng, Y. Jiang and Y.H. Huang, *Adv. Mater.*, 26 (2014) 6622.
18. N.N. Wang, H.Y. Xu, L. Chen, X. Gu, J. Yang and Y.T. Qian, *J. Power Sources*, 247 (2014) 163.
19. H.Y. Xu, X.L. Chen, L. Chen, L. Li, L.Q. Xu, J. Yang and Y.T. Qian, *Int. J. Electrochem. Sci.*, 7 (2012) 7976.